Nanoscale

PAPER

View Article Online
View Journal | View Issue

Cite this: *Nanoscale*, 2024, **16**, 14378

Assembling Fe_4 single-molecule magnets on a TiO_2 monolayer†

Andrea Luigi Sorrentino, [a,b] Lorenzo Poggini, *[b,c] Giulia Serrano, [a,b] Giuseppe Cucinotta, [b] Brunetto Cortigiani, [b] Luigi Malavolti, [d] Francesca Parenti, [e] Edwige Otero, [f] Marie-Anne Arrio, [g] Philippe Sainctavit, [f,g] Andrea Caneschi, [a] Andrea Cornia, [e] Roberta Sessoli [b,c] and Matteo Mannini *[b]

The decoration of technologically relevant surfaces, such as metal oxides, with Single-Molecule Magnets (SMMs) constitutes a persistent challenge for the integration of these molecular systems into novel technologies and, in particular, for the development of spintronic and quantum devices. We used UHV thermal sublimation to deposit tetrairon(III) propeller-shaped SMMs (Fe_4) as a single layer on a TiO_2 ultrathin film grown on Cu(001). The properties of the molecular deposit were studied using a multi-technique approach based on standard topographic and spectroscopic measurements, which demonstrated that molecules remain largely intact upon deposition. Ultralow temperature X-ray Absorption Spectroscopy (XAS) with linearly and circularly polarized light was further employed to evaluate both the molecular organization and the magnetic properties of the Fe_4 monolayer. X-ray Natural Linear Dichroism (XNLD) and X-ray Magnetic Circular Dichroism (XMCD) showed that molecules in a monolayer display a preferential orientation and an open magnetic hysteresis with pronounced quantum tunnelling steps up to 900 mK. However, unexpected extra features in the XAS and XMCD spectra disclosed a minority fraction of altered molecules, suggesting that the TiO_2 film may be chemically non-innocent. The observed persistence of SMM behaviour on a metal oxide thin film opens new possibilities for the development of SMM-based hybrid systems.

Received 27th May 2024,
Accepted 1st July 2024

DOI: 10.1039/d4nr02234c

rsc.li/nanoscale

Introduction

Single-Molecule Magnets (SMMs) are extremely promising building blocks for the development of molecular spintronic and quantum computing applications because of their magnetic bistability and unique quantum behavior.[1–8] In this context, the assembling of SMMs on solid substrates is a key step for developing breakthrough technological devices.[9–12] The persistence of SMM properties on a surface, including magnetic hysteresis and Quantum Tunneling of the Magnetization (QTM), was demonstrated in 2009 by sub-kelvin measurements.[13,14] Since then, the operating temperature of surface-supported SMMs has increased considerably and the current record is 28 K for $Tb_2@C_{80}(CH_2Ph)$ assembled on graphene.[15] More recently, the focus has moved to "active" substrates as a means to either directly control molecular quantum dynamics (*e.g.* superconductors),[16,17] enhance SMM performances,[18,19] or facilitate single-spin sensing.[20–23] Thin decoupling layers of metal oxides, such as MgO, were found to dramatically enhance the magnetic remanence of $TbPc_2$ SMM films (H_2Pc = phthalocyanine).[18,19] MgO layers[20,21,24–26] were also crucial for sensing the local magnetic features of molecules or atoms by Scanning Tunneling Microscopy (STM),[20,25,27,28] allowing the STM detection of EPR-like signals from paramagnetic species.[20,27,29,30]

The vastness of available oxide materials and their widespread use for technological applications leaves additional space for the exploration of alternative materials which can support molecular spin functionalities. In this context, TiO_2

[a]*Department of Industrial Engineering - DIEF - and INSTM Research Unit, University of Florence, Via Santa Marta 3, 50139 Florence, Italy*
[b]*Department of Chemistry "U. Schiff" - DICUS - and INSTM Research Unit, University of Florence, Via della Lastruccia 3-13, 50019 Sesto Fiorentino, FI, Italy. E-mail: lpoggini@iccom.cnr.it, matteo.mannini@unifi.it*
[c]*Institute for Chemistry of Organo-Metallic Compounds (ICCOM-CNR), Via Madonna del Piano, 50019 Sesto Fiorentino, FI, Italy*
[d]*Max Planck Institute for Solid State Research, Heisenbergstr. 1, 70569 Stuttgart, Germany*
[e]*Department of Chemical and Geological Sciences and INSTM Research Unit, University of Modena and Reggio Emilia, Via G. Campi 103, 41125 Modena, Italy*
[f]*Synchrotron-SOLEIL, L'Orme des Merisiers, 91192 Saint-Aubin, France*
[g]*CNRS UMR7590, Institut de Minéralogie, de Physique des Matériaux et de Cosmochimie (IMPMC), Sorbonne Université/MNHN, 4 place Jussieu, 75252 Paris Cedex 5, France*

† Electronic supplementary information (ESI) available. See DOI: https://doi.org/10.1039/d4nr02234c

has a high technological significance thanks to its photocatalytic[31,32] and electron transport properties,[33,34] which are of relevance for sensing,[35] catalysis, and photovoltaics.[36–38] The nature of the surface plays a decisive role in promoting these functionalities, and the richness of TiO_2 structural phases that are accessible by finely tuning the preparation technique makes this material particularly versatile for multifunctional electronic devices.[39] In fact, TiO_2 can be nanostructured as a thin film grown on metals to control its electronic properties,[40–42] which depend on the structural phase, the surface stoichiometry, and the presence of defects.[43–45] For instance, some of us demonstrated that Cu(001) surface is a good playground for the growth of continuous TiO_2 films having different structural phases and electronic properties depending on growth condition parameters.[46] In parallel, we showed that SMM behaviour of $TbPc_2$ molecules might persist on sub-monolayer TiO_2 islands with a lepidocrocite-like structure grown on Ag(100).[47]

Here, we investigated the chemical, structural, and magnetic properties of tetrairon(III) propeller-like SMMs (Fe_4) deposited on a single layer of TiO_2 grown on Cu(001) (hereafter called TiO_2/Cu). The Fe_4 complexes are archetypal, low-temperature SMMs with general formula $[Fe_4(L^R)_2(dpm)_6]$, where a central Fe^{III} ion is surrounded by three peripheral Fe^{III} ions arranged at the vertices of a triangle. The dipivaloylmethanido ligands (dpm^-) bind exclusively to peripheral ions, while the magnetic core is held together by two tripodal ligands $(L^R)^{3-}$ = $[RC(CH_2O)_3]^{3-}$. The bridging oxygen atoms of the tripods promote antiferromagnetic interactions between the s = 5/2 spins of the central and peripheral Fe^{III} ions, yielding a molecular spin S = 5 ground state.[48] Complexes of this family exhibit slow magnetic relaxation only below 1 K, but have good chemical stability and can be easily functionalized by proper choice of the R substituent. In this way, derivatives suitable for deposition on surfaces by either a wet-chemistry approach, electrospray, or thermal sublimation in UHV have been designed.[13,14,16,49–54] Recently, a Fe_4 derivative with R = CH_2SMe (hereafter called Fe_4SMe) was sublimated on Pb(111), showing great chemical stability and enhanced organization on the surface promoted by the short S-functionalized tethering group.[16] This derivative was indeed originally designed for deposition on metal surfaces (*e.g.*, Au, Pb) to form a well-ordered and assembled monolayer. Although it is not specifically tailored for TiO_2 substrates, it exhibits superior stability during thermal sublimation and improved magnetic behavior compared to all other Fe_4 compounds.[51,55]

In this paper, we deposited Fe_4SMe molecules on the TiO_2/Cu surface and used both STM and X-ray Photoelectron Spectroscopy (XPS) to check their chemical and structural integrity after deposition. Furthermore, we used synchrotron-based X-ray Absorption Spectroscopy (XAS) methods, namely X-ray Natural Linear Dichroism (XNLD) and X-ray Magnetic Circular Dichroism (XMCD), to probe their electronic structure and magnetic properties. This spectroscopic study showed that the main fraction of Fe_4SMe complexes are intact and feature magnetic hysteresis and QTM up to 900 mK, while a minority fraction of molecules contain reduced Fe^{II} metal centers and become paramagnetic.

Results and discussion

The TiO_2 film was grown on Cu(001) single crystal (see Methods) and studied by XPS and STM to get chemical, morphological, and structural information. The Ti 2p XPS spectrum, reported in Fig. 1a, reflects an estimated coverage of 1 ML. It is dominated by the expected Ti^{IV} signal at 458.7 eV (Ti $2p_{3/2}$)[46,56] and by its spin–orbit coupled component (Ti $2p_{1/2}$) shifted by 5.7 eV (Fig. 1a, in light magenta).[46,57] Shake-up components are present at higher binding energies (460.8 and 466.5 eV, Fig. 1a, in wine) along with satellite features at 471.8 and 482.5 eV (Fig. 1a, in green).[46,58–60] Furthermore, an

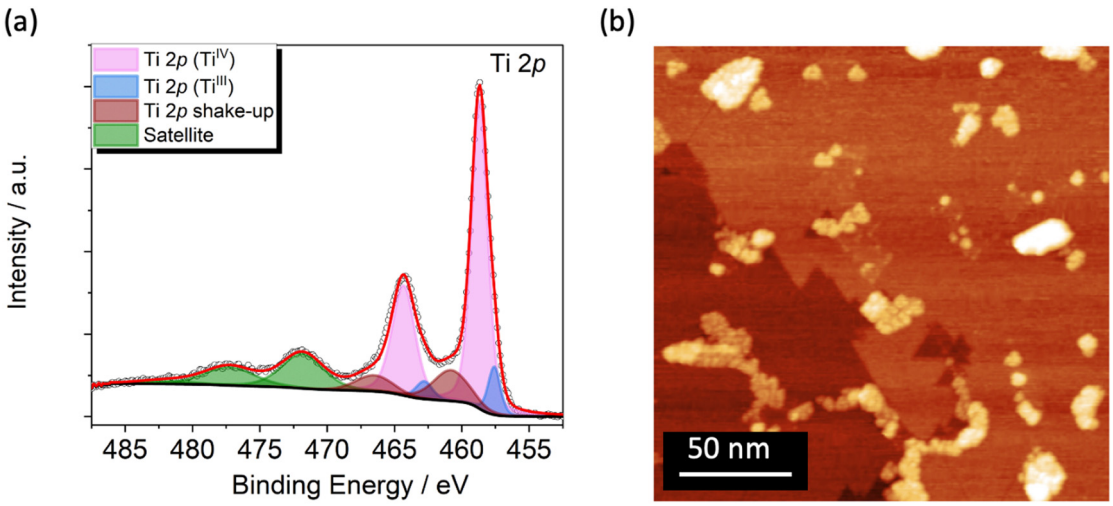

Fig. 1 (a) Ti 2p XPS spectrum of the TiO_2 single layer grown on Cu(001) single crystal. (b) STM image of the TiO_2/Cu surface at RT (V = 1.5 V, It = 150 pA).

additional component located at 457.6 eV, accompanied by its spin–orbit coupled peak, discloses a small amount of Ti^{III} arising from the reductive annealing process (Fig. 1a, in blue).[61–64] From the deconvolution analysis of the spectra this reduced fraction amounts to 10.5% of the overall titanium content (see Fig. S3 and Table S1†). The signals in the O 1s XPS spectrum (Fig. S1†) are typical for TiO_2 films[46,62,64] and are discussed in detail in the XPS characterization section of the ESI.†

STM images at Room Temperature (RT) were acquired to evaluate the film morphology and to confirm the TiO_2 coverage estimated by XPS. The wide-area image in Fig. 1b shows a complete layer of TiO_2, characterized by domain boundaries that suggest the presence of the quasi-hexagonal (**QH**) structure with squared bright spot ascribable to the growth of a second TiO_2 layer.[46] The formation of the single layer of TiO_2-**QH** grown on Cu(001) structure is confirmed by Low Energy Electron Diffraction (LEED) showing two $p(2 \times 7)$ domains rotated by 30 degrees (Fig. S2†).[46,65,66]

A monolayer of Fe_4SMe was deposited on TiO_2/Cu following the protocol described in Methods. After molecular deposition, the XPS spectrum in the Ti 2p region (Fig. S3†) shows no significant variation as compared with that of the pristine substrate, thus confirming the stability of the TiO_2 surface upon further processing.[47,64,67] The small decrease (0.3%) of the Ti^{III} fraction lies well within the limits of semiquantitative analysis by XPS (Table S1†). The C 1s spectrum reported in Fig. 2a reveals two main contributions attributed to the aliphatic and oxygen-bound carbon atoms of the molecular layer at 284.9 and 286.5 eV (Fig. 2a, in yellow and dark blue, respectively). An additional shake-up component is present at 289.6 eV (Fig. 2a, in cyan).[16,68] The S 2p signal consists in two contributions located at 163.7 eV and at 164.9 eV (spin–orbit coupled component) (Fig. 2b), indicating the presence of intact CH_2SMe functional groups.[69–71] The C/S atomic ratio (46.0 ± 2.3) is in gross agreement with the expected value of 39 based on the molecular formula ($C_{78}H_{136}Fe_4O_{18}S_2$), and suggests the overall integrity of Fe_4SMe molecules on the TiO_2/Cu surface. Unfortunately, a more comprehensive semiquantitative elemental analysis of the molecular species cannot be carried out due to the overlap of the molecular Fe 2p and O 1s signals with the Cu LMM Auger

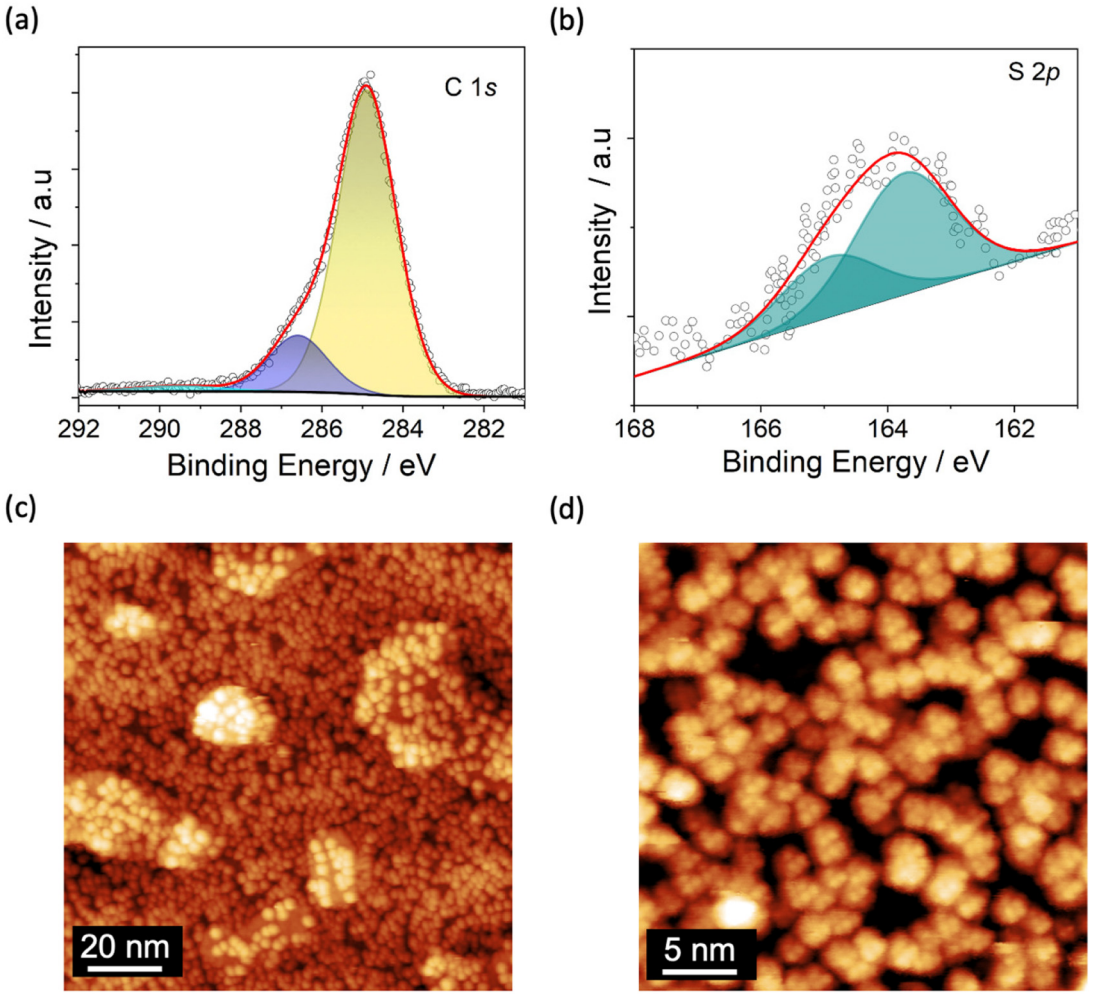

Fig. 2 XPS spectra in the C 1s (a) and S 2p (b) regions after deposition of Fe_4SMe on TiO_2/Cu surface. (c) STM image at 30 K of Fe_4SMe molecules distributed randomly on the TiO_2/Cu surface (V = 2.6 V, It = 15 pA, 120 × 120 nm). (d) STM image at 30 K of the Fe_4SMe layer showing the internal resolution (yellow dots) of single molecules (V = 2.6 V, It = 5 pA, 30 × 30 nm).

peaks and the oxygen signals, respectively, of the TiO_2/Cu substrate.[46,72] However, successful sublimation of Fe_4SMe molecules has been demonstrated in a previous study.[16]

STM images of the TiO_2/Cu surface decorated with Fe_4SMe molecules acquired at 30 K and different magnifications are displayed in Fig. 2c and d. An almost complete coverage of the surface by Fe_4SMe molecules is clearly visible. Molecules have a quasi-spherical shape but do not form densely packed and ordered islands, as observed on metals.[16] Uncovered parts of the TiO_2 surface and a few additional molecules sitting on top of the molecular film are visible, confirming that the desired monolayer coverage was reached. The statistical height distribution in the Fe_4SMe monolayer is shown in Fig. S4† and provides a medium height of 0.65 ± 0.06 nm. This value is slightly lower than that observed for the same Fe_4 derivative on Pb(111)[16] and for the related complex with R = Ph (Fe_4Ph) on Au(111)[51] and Cu_2N[22] (~0.8 nm). Such a slightly reduced molecular height could be attributed either to a different molecular orientation or to a stronger molecule/surface interaction, which would be consistent with the absence of dense and ordered molecular packing. Furthermore, within the limits of our STM investigation, the presence of molecular fragments can be excluded, confirming the enhanced stability of Fe_4SMe[16] *vs.* Fe_4Ph[51,55] upon sublimation.

From the STM image at higher magnification (Fig. 2d) we estimated a lateral dimension of 1.80 ± 0.15 nm for individual molecules (Fig. S5†), a value in close agreement with the X-ray structure (1.7 nm) and consistent with literature data for Fe_4 complexes on other surfaces.[22,48,51] Additionally, the STM image in Fig. 2d evidences the internal resolution of single Fe_4 units, with a triangle of bright features separated by 0.58 ± 0.06 nm (see line profile in Fig. S5a and S5b†). These features are similar to those observed on Pb(111)[16] and can be attributed to the $-CH_2SMe$ group pointing out of the plane, a *tert*-butyl group of the topmost dpm^- ligand, and the surrounding envelope of dpm^- ligands.

The electronic and magnetic properties of the Fe_4SMe deposit were investigated by synchrotron radiation at the DEIMOS beamline (SOLEIL, France) using a dilution cryostat to reach sub-kelvin temperatures.[73] These experiments were carried out with linearly and circularly polarized light (Fig. 3) by monitoring the absorption at the Ti $L_{2,3}$ and Fe $L_{2,3}$ edges in the Total Electron Yield detection mode (TEY). Experiments were performed between 220 and 900 mK and in magnetic fields up to 30 kOe (see Methods). The XAS profile at the Ti $L_{2,3}$ edges confirms the **QH** structure of the TiO_2 monolayer deposited on Cu (see ESI and Fig. S6† for additional details). The XAS spectrum at the Fe L_3 edge exhibits a fine structure with two main signals at 707.6 and 709.2 eV (Fig. 3a). We notice that the first peak has an additional shoulder approximately centered at 707.1 eV and marked with a green arrow in Fig. 3a. This extra XAS component was not detected in our previous investigations of Fe_4 arrays at surfaces.[16,51,74,75] Significantly, it was absent in monolayers of the same Fe_4SMe complex prepared using identical thermal sublimation conditions but a different substrate.[16] Therefore, the thermal sublimation process is unlikely to be responsible for this feature.[55] Radiation damage is ruled out as a possible cause of the XAS profile alteration, since there is no evidence of time evolution of this feature under X-ray irradiation.[71,76,77] A plausible explanation is the partial reduction of molecules interacting with Ti^{III} sites on the TiO_2 surface to give a minority fraction of Fe^{II} containing species[55,64,78,79] and this aspect will be the subject of further discussion later.

The XNLD contribution (Fig. 3a) was extracted from the XAS signals recorded using linearly polarized X-rays with propagation vector directed at θ = 45° from the surface normal (see Methods and inset in Fig. 3a). The overall XNLD profile is essentially in line with that reported earlier for other Fe_4 derivatives with short tethering groups.[14,16,75] From the maximum XNLD amplitude, which reaches 6% of the average isotropic XAS signal, we conclude that the extent of preferential orientation on the surface is similar to that found for the same complex on Pb(111).[16]

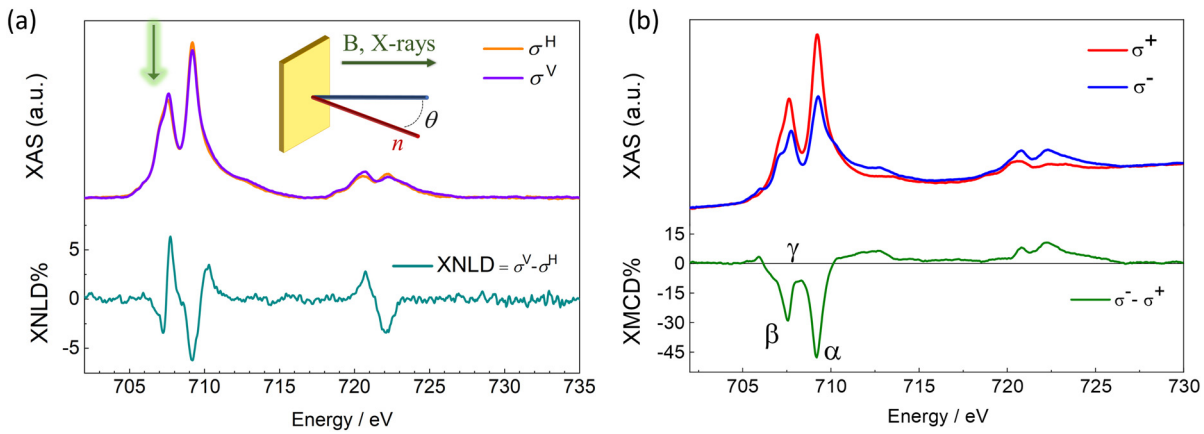

Fig. 3 (a) XNLD and (b) XMCD spectra of Fe_4SMe on TiO_2/Cu acquired at the Fe $L_{2,3}$ edges. (a) XAS (top) and XNLD (bottom) spectra recorded at θ = 45°, H = 30 kOe, and T = 220 mK. (b) XAS (top) and XMCD (bottom) spectra recorded at θ = 0, H = 30 kOe, and T = 220 mK. The inset in panel (a) depicts the experimental geometry used for the acquisition of the XAS spectra. The green arrow indicates the additional contribution at 707.1 eV, which is observable for all polarization, attributed to a minority fraction of Fe(II) containing species.

The XMCD profile (Fig. 3b), obtained from the XAS signals recorded using circularly polarized X-rays at 220 mK and $\theta = 0$, is dominated by two negative dichroic signals at the L_3 edge. Although the position of the two XMCD minima (707.6 and 709.2 eV, β and α, respectively) agrees with that typically observed in Fe_4 complexes, the exact shape and amplitude of the XMCD profile are slightly different. In the ground $S = 5$ state of Fe_4 complexes, the opposing contribution of the central Fe^{III} spin results in three important spectral fingerprints:[16,48,51,74,75,80,81] (i) an intensity ratio of *ca.* 0.30 between the two XMCD minima at the L_3 edge, (ii) saddle point between the two intense negative signals (708.3 eV, γ), and (iii) a maximum XMCD amplitude amounting to *ca.* 40% of the average isotropic XAS signal. In Fig. 3b, the intensity ratio between the two XMCD minima at the L_3 edge is 0.55, hence higher than typically found in Fe_4 complexes. In addition, the XMCD signal at 708.3 eV (−8%) remains significantly different from zero, and the normalized XMCD intensity at 709.2 eV is as large as 47%. It is worth stressing that heteronuclear Cr^{III}-centered Fe_3Cr complexes, in which the opposing spin contribution of the central Fe^{III} ion is absent, also exhibit a non-zero XMCD signal at 708.3 eV and a much increased XMCD amplitude at 709.2 eV.[74,80] Here, the Fe_4 spectral fingerprints are presumably partly obscured by the surface-induced reduction of some Fe^{III} centers to Fe^{II}.

To support this interpretation of the XMCD fine structure, we performed Ligand Field Multiplet (LFM) calculations. Starting from our previous knowledge of the XAS and XMCD signals for pristine Fe_4 molecules, we replaced Fe^{III} with variable amounts of Fe^{II} in the calculations. We reached a good agreement with the measured XAS spectra assuming that 30% of the Fe centers are reduced to Fe^{II}. With this percentage, the ratio between the first peak at 707.6 eV and the main peak at 709.2 eV in the XAS plots is nicely reproduced (Fig. S7†). In order to determine the speciation of Fe^{II}, we examined various situations where the amount of Fe^{II} was fixed to 30% of the total Fe ion content. It should be underlined that if one supposes that all the Fe^{II} ions are present as Fe oxyhydroxides at the TiO_2 surface, the XMCD signal at 220 mK and 30 kOe would be much larger than measured. Thus, one can exclude this situation as the main location for Fe^{II} ions and suppose that Fe^{II} ions primarily occur in the Fe_4 molecular structure. There are only five distinct distributions of oxidation states which are compatible with a 30% concentration of Fe^{II} ions, as fully detailed in the ESI (see Fig. S7†). Among these five different distributions, the one with 70% of pristine Fe_4 molecules and 30% of Fe_4^{II} molecules yields by far the best agreement with the measured XAS and XMCD signals. Note that in the present fit we always considered that the central ion, whether it is an Fe^{II} or an Fe^{III} ion, is coupled antiferromagnetically with the three peripheral Fe ions (see ESI† for the precise values of the Fe^{II} LFM parameters). The resulting simulation features an intensity ratio of ≈0.51 between the two XMCD minima at the L_3 edge, a normalized XMCD intensity of ≈50% at 709.2 eV, and a negative XMCD signal of −4% at 708.3 eV. The three above features rather closely match the experimental spectra, strongly supporting the presence of a fraction of Fe^{II} ions in the molecular deposit, which however primarily comprises intact Fe_4SMe molecules. An additional and strong indication that the monolayer contains a fraction of altered molecules was extracted by monitoring the magnetic field dependence of the XMCD signal at different energies to selectively address the magnetic behaviour of the different species on the surface. We expect that intact Fe_4SMe molecules mainly contribute to the XMCD signal at 709.2 eV, and not at 708.3 eV. The temperature dependence of XMCD at 709.2 eV (α, Fig. 4a) mirrors the typical magnetic behaviour of Fe_4 SMMs, whose hysteresis loop is open below 1 K and becomes wider with decreasing temperature.[48] In particular, the sharp magnetization steps at 0 and 5 kOe show that Fe_4SMe undergoes resonant QTM on TiO_2/Cu, similarly to what has been observed on Pb(111).[16] Additionally, in agreement with XNLD evidence, the angular-dependent experiment at 220 mK (Fig. 4b) confirms that the complex is preferentially oriented with the easy axis close to the surface normal. As the incidence angle θ increases, saturation is reached more slowly and the resonant condition for QTM at a nonzero field broadens and shifts to higher fields.[1451]

When the photon energy is decreased to 708.3 eV (γ), the intensity of the XMCD signal at 220 mK decreases considerably, primarily due to the contribution of the reduced species only (Fig. 4c). Crucially, its field dependence is markedly different from that of Fig. 4b, evidencing a closed hysteresis loop. We attribute this paramagnetic response at 708.3 eV to magnetic species containing Fe^{II} centres resulting from surface-induced reduction but still embedded in a Fe_4-like structure, in accordance with STM measurements and LFM calculations. For the sake of completeness, setting the photon energy at 707.6 eV (β) yields a field-dependent XMCD signal with intermediate characteristics as compared with those recorded at 709.2 (α) and 708.3 (γ) eV. In this case, the hysteresis loop is still detectable but smeared out due to the additional paramagnetic contribution.

To summarize, our combined spectroscopic studies by XAS, XNLD, and XMCD converge in indicating that Fe_4SMe monolayers on TiO_2/Cu contain a dominant fraction of intact molecules and a minor fraction of molecules undergoing significant modification. XAS spectra suggest that such a modification consists of a reduction of Fe^{III} centers to Fe^{II}. Theoretical calculations already predicted a similar effect for atoms on TiO_2.[82] A strong molecule–surface interaction was also observed when mono and bis-phthalocyaninato complexes are deposited on TiO_2,[64,79,83–86] leading in extreme circumstances to surface–molecule charge transfer processes.[64,86–88] The latter could be favoured by TiO_2 reactive sites, such as oxygen vacancies.[89] We can tentatively associate the partial modification of Fe_4SMe complexes on TiO_2/Cu with the presence of Ti^{III} active sites on the surface. Considering the overwhelming number of Ti^{III} atoms compared to Fe_4SMe molecules, such a hypothesis does not contradict the observation that the amount of Ti^{III} remains substantially unaltered after Fe_4SMe deposition (Fig. S3 and Table S1†).

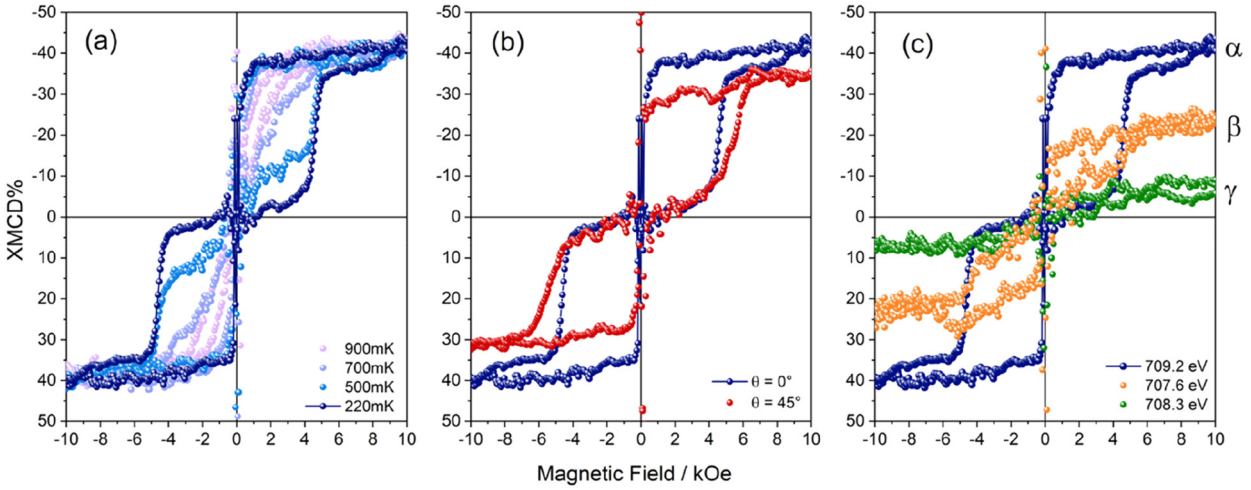

Fig. 4 Magnetic field-dependent XMCD curves acquired (a) as a function of temperature at 709.2 eV and normal incidence (θ = 0), (b) as a function of θ at 709.2 eV and 220 mK, and (c) as a function of photon energy at normal incidence and 220 mK (magnified from −10 to 10 kOe). All data were obtained at the same field sweep rate of 0.2 kOe s^{-1}. The measurements at 220 mK, θ = 0°, E = 709.2 eV are plotted as dark blue dots with connecting line in (a), (b) and (c) and compared with the other measurements where one parameter (temperature (a), angle (b) and energy (c)) is varied.

Conclusions

We reported the chemical, structural, and magnetic properties of a monolayer of Fe_4SMe complexes sublimated on an ultrathin film of TiO_2-**QH** grown on Cu(001). The XPS and STM measurements evidenced the presence of chemically and structurally intact Fe_4SMe molecules assembled into a disordered monolayer. This might imply that a significant molecule/surface interaction occurs, as previously observed for other molecules on TiO_2 surfaces.[47,64] An ultralow-temperature investigation by XNLD and XMCD at the Fe $L_{2,3}$ edges revealed that Fe_4SMe molecules display a preferential orientation in the monolayer and retain a bulk-phase-like behaviour (*i.e.*, magnetic hysteresis up to 900 mK). However, the XAS spectra and the energy- and field-dependent XMCD signal disclosed a minor contribution from altered species containing Fe^{II} ions. These reduced species may originate from the reaction of Fe_4SMe with active sites in the TiO_2 monolayer, which hosts a detectable amount of Ti^{III} ions. Additional experiments aimed at modifying the Ti^{III} content and future DFT investigations will be required to clarify this aspect. Interestingly, the possibility to selectively address at the monolayer level the magnetic properties of the altered species combined with the SMM fingerprint can provide information on the underlying interface, as already observed for the intermediate superconducting state of a Pb substrate.[16] Overall, our findings highlight the challenges associated with combining 2D oxide materials with SMM complexes into hybrid architectures suitable for new spintronic and quantum devices.

Methods

A Cu(001) single crystal from the Surface Preparation Laboratory (SPL, The Netherlands) was cleaned by several cycles of Ar^+ sputtering (1500 eV) and annealing (770 K) in UHV. The Cu(001) substrate, kept at the constant temperature of 570 K, was exposed to an oxygen partial pressure of ≈1 × 10^{-6} mbar to provide the oxygen amount necessary for growing the first TiO_2 layer. Finally, titanium (purity 99.999%) was deposited employing an electron beam Omicron EFM3 micro-evaporator. The TiO_2 deposition was achieved by consecutive steps following the procedure reported in the literature.[46] After each step, the Cu(001) single crystal was annealed at *ca.* 700 K to promote a homogeneous growth on the metal surface. The deposition rate was monitored using the integrated flux monitor of the EFM3 and evaluated *a posteriori* by STM. The structure and the chemical composition of the TiO_2 layer were studied by LEED and XPS, respectively. The Fe_4SMe complex, prepared in pure crystalline form as reported elsewhere,[16] was processed as described for deposition on Pb(111).[16] It was heated at a temperature of around 490 K and evaporated with a homemade Knudsen cell in an UHV chamber (with a base pressure of 10^{-9} mbar). Molecular coverage was estimated by a Quartz Crystal Microbalance (QCM) and by STM measurements. The deposition rate was monitored by placing the QCM in front of the crucible. The molecular integrity after deposition was investigated by XPS. XPS data were acquired using a micro-focused monochromatic Al Kα radiation (λ = 1486.6 eV, SPECS mod. XR-MS focus 600) operating at a power of 100 W (13 kV and 7.7 mA) and a multichannel detector electron analyser, model SPECS Phoibos 150 1DLD. XPS spectra were recorded in normal emission with pass energy of 40 eV with the X-ray source mounted at an angle of 54.44° with respect to the analyser. XPS spectra were calibrated to the Cu $2p_{3/2}$ signal at 932.7 eV,[46] and the background subtracted was adapted as a function of the elements, employing linear and Shirley method. A 70%–30% combination of Gaussian and Lorentzian functions was employed to fit all the spectra. LEED patterns were acquired using an

Omicron three grid optics, model NG-LEED. STM measurements were carried out in UHV conditions at RT and at 30 K using a Variable Temperature (VT)-STM Omicron (model XA VT-STM) with a Pt/Ir tip.

The electronic and magnetic characterization of the Fe_4SMe complex on TiO_2/Cu was carried out at the DEIMOS beamline (SOLEIL synchrotron).[73,90] The XNLD was extracted as the difference between the cross sections recorded using vertically (σ^V) and horizontally (σ^H) polarized light ($\sigma^V - \sigma^H$) at $\theta = 45°$, $H = 30$ kOe, and $T = 220$ mK. The XNLD contribution was normalized with respect to the L_3 edge jump of the isotropic spectrum ($1/3\sigma^V + 2/3\sigma^H$) and expressed as percentage (XNLD%). Analogously, XMCD was obtained as the difference between the XAS spectra measured using negative (σ^-) and positive (σ^+) circular light polarizations ($\sigma^- - \sigma^+$) at $\theta = 0$, $H = 30$ kOe, and $T = 220$ mK. The dichroic signal was normalized with respect to the L_3 edge jump of $(\sigma^+ + \sigma^-)/2$ and expressed as percentage (XMCD%). The magnetic hysteresis measurements at specific photon energies were made at $\theta = 0$ or 45° by cycling the magnetic field between −15 kOe and 15 kOe with a scan rate of 0.2 kOe s^{-1} and working at temperatures from 220 to 900 mK. All the samples were prepared in Florence and transferred to the beamline employing a home-made suitcase equipped with a D100 SAES Nextorr Neg-Ion Combination Pump that guarantees a pressure $P < 10^{-10}$ mbar during the transport. All the steps from sample preparation to synchrotron measurements were accomplished without breaking the vacuum connection ($P < 10^{-9}$ mbar).[16] Data analysis was performed using pyDichroX software.[91]

The XAS and XMCD spectra were calculated within the Ligand Field Multiplet (LFM) theory using Quanty[92] (see ESI† for details).

Author contributions

A. L. S. – formal analysis, investigation (XPS, STM, large scale facilities experiments), writing – original draft; L. P. – formal analysis, investigation (XPS, large scale facilities experiments), supervision data discussion, writing – review & editing, data curation; G. S. – supervision, formal analysis, investigation (STM, large scale facilities experiments), data discussion, writing – review & editing; G. C. – investigation (large scale facilities) and software development; B. C. – technical assistance; L. M. – investigation (large scale facilities); F. P. investigation (synthesis); E. O. – investigation (large scale facilities) and technical assistance; M.-A. A. – data discussion and investigations (simulations); P. S. – data discussion and investigations (simulations); A. C. – supervision; A. Co. – conceptualization, investigation (synthesis); R. S. – conceptualization, funding acquisition, project administration, supervision, validation, writing – review & editing; M. M. – conceptualization, funding acquisition, project administration, supervision, validation, writing – review & editing, investigation (large scale facilities experiments).

Data availability

Figures for this article are available at Zonodo repository website at **https://doi.org/10.5281/zenodo.12598761**.

Conflicts of interest

There are no conflicts to declare.

Acknowledgements

We are grateful to the SOLEIL staff for smoothly running the facility. The work was supported by MUR Italy through the program Dipartimenti di Eccellenza 2023–2027 (DICUS 2.0 grant, assigned to the Department of Chemistry "Ugo Schiff" of the University of Florence, CUP: B97G22000740001) and a PNRR project (PE0000023-NQSTI). Financing by the Fondazione Ente Cassa di Risparmio di Firenze (project SPINE-2 2020.1634) and by ANR France (LabEx PALM project, ANR-10-LABX-0039-PALM) is also acknowledged. We thank the MatchLab Interdepartment Research Unit (Univ. of Florence). We acknowledge SOLEIL synchrotron (proposal #99180040 test) and DEIMOS Staff.

References

1 R. Sessoli, D. Gatteschi, A. Caneschi and M. A. Novak, *Nature*, 1993, **365**, 141–143.
2 R. Clérac and R. E. P. Winpenny, *Struct. Bonding*, 2016, **172**, 35–48.
3 L. Bogani and W. Wernsdorfer, *Nat. Mater.*, 2008, **7**, 179–186.
4 C. A. Gould, K. R. McClain, D. Reta, J. G. C. Kragskow, D. A. Marchiori, E. Lachman, E.-S. Choi, J. G. Analytis, R. D. Britt, N. F. Chilton, B. G. Harvey and J. R. Long, *Science*, 2022, **375**, 198–202.
5 F.-S. Guo, B. M. Day, Y.-C. Chen, M.-L. Tong, A. Mansikkamäki and R. A. Layfield, *Science*, 2018, **362**, 1400–1403.
6 F.-S. Guo, B. M. Day, Y.-C. Chen, M.-L. Tong, A. Mansikkamäki and R. A. Layfield, *Angew. Chem., Int. Ed.*, 2017, **56**, 11445–11449.
7 C. A. P. Goodwin, F. Ortu, D. Reta, N. F. Chilton and D. P. Mills, *Nature*, 2017, **548**, 439–442.
8 D. Gatteschi, R. Sessoli and J. Villain, *Molecular Nanomagnets*, Oxford University Press, 2006, vol. 54.
9 E. Coronado, *Nat. Rev. Mater.*, 2020, **5**, 87–104.
10 D. Shimizu and A. Osuka, *Chem. Sci.*, 2018, **9**, 1408–1423.
11 C. A. P. Goodwin, F. Ortu, D. Reta, N. F. Chilton and D. P. Mills, *Nature*, 2017, **548**, 439–442.
12 F. Guo, B. M. Day, Y. Chen, M. Tong, A. Mansikkamäki and R. A. Layfield, *Angew. Chem., Int. Ed.*, 2017, **56**, 11445–11449.

13 M. Mannini, F. Pineider, P. Sainctavit, C. Danieli, E. Otero, C. Sciancalepore, A. M. Talarico, M.-A. Arrio, A. Cornia, D. Gatteschi and R. Sessoli, *Nat. Mater.*, 2009, **8**, 194–197.
14 M. Mannini, F. Pineider, C. Danieli, F. Totti, L. Sorace, P. Sainctavit, M.-A. Arrio, E. Otero, L. Joly, J. C. Cezar, A. Cornia and R. Sessoli, *Nature*, 2010, **468**, 417–421.
15 L. Spree, F. Liu, V. Neu, M. Rosenkranz, G. Velkos, Y. Wang, S. Schiemenz, J. Dreiser, P. Gargiani, M. Valvidares, C.-H. Chen, B. Büchner, S. M. Avdoshenko and A. A. Popov, *Adv. Funct. Mater.*, 2021, **31**, 2105516.
16 G. Serrano, L. Poggini, M. Briganti, A. L. Sorrentino, G. Cucinotta, L. Malavolti, B. Cortigiani, E. Otero, P. Sainctavit, S. Loth, F. Parenti, A.-L. L. Barra, A. Vindigni, A. Cornia, F. Totti, M. Mannini and R. Sessoli, *Nat. Mater.*, 2020, **19**, 546–551.
17 G. Serrano, L. Poggini, G. Cucinotta, A. L. Sorrentino, N. Giaconi, B. Cortigiani, D. Longo, E. Otero, P. Sainctavit, A. Caneschi, M. Mannini and R. Sessoli, *Nat. Commun.*, 2022, **13**, 3838.
18 C. Wäckerlin, F. Donati, A. Singha, R. Baltic, S. Rusponi, K. Diller, F. Patthey, M. Pivetta, Y. Lan, S. Klyatskaya, M. Ruben, H. Brune and J. Dreiser, *Adv. Mater.*, 2016, **28**, 5195–5199.
19 M. Studniarek, C. Wäckerlin, A. Singha, R. Baltic, K. Diller, F. Donati, S. Rusponi, H. Brune, Y. Lan, S. Klyatskaya, M. Ruben, A. P. Seitsonen and J. Dreiser, *Adv. Sci.*, 2019, **6**, 1901736.
20 X. Zhang, C. Wolf, Y. Wang, H. Aubin, T. Bilgeri, P. Willke, A. J. Heinrich and T. Choi, *Nat. Chem.*, 2022, **14**, 59–65.
21 F. Donati, S. Rusponi, S. Stepanow, L. Persichetti, A. Singha, D. M. Juraschek, C. Wäckerlin, R. Baltic, M. Pivetta, K. Diller, C. Nistor, J. Dreiser, K. Kummer, E. Velez-Fort, N. A. Spaldin, H. Brune and P. Gambardella, *Phys. Rev. Lett.*, 2020, **124**, 077204.
22 J. A. J. Burgess, L. Malavolti, V. Lanzilotto, M. Mannini, S. Yan, S. Ninova, F. Totti, S. Rolf-Pissarczyk, A. Cornia, R. Sessoli and S. Loth, *Nat. Commun.*, 2015, **6**, 8216.
23 A. J. Heinrich, W. D. Oliver, L. M. K. Vandersypen, A. Ardavan, R. Sessoli, D. Loss, A. B. Jayich, J. Fernandez-Rossier, A. Laucht and A. Morello, *Nat. Nanotechnol.*, 2021, **16**, 1318–1329.
24 S. Loth, K. von Bergmann, M. Ternes, A. F. Otte, C. P. Lutz and A. J. Heinrich, *Nat. Phys.*, 2010, **6**, 340–344.
25 S. Baumann, W. Paul, T. Choi, C. P. Lutz, A. Ardavan and A. J. Heinrich, *Science*, 2015, **350**, 417–420.
26 W. Paul, K. Yang, S. Baumann, N. Romming, T. Choi, C. P. Lutz and A. J. Heinrich, *Nat. Phys.*, 2017, **13**, 403–407.
27 F. Donati and A. J. Heinrich, *Appl. Phys. Lett.*, 2021, **119**, 160503.
28 P. Willke, Y. Bae, K. Yang, J. L. Lado, A. Ferrón, T. Choi, A. Ardavan, J. Fernández-Rossier, A. J. Heinrich and C. P. Lutz, *Science*, 2018, **362**, 336–339.
29 J. Kim, K. Noh, Y. Chen, F. Donati, A. J. Heinrich, C. Wolf and Y. Bae, *Nano Lett.*, 2022, **22**, 9766–9772.
30 P. Willke, T. Bilgeri, X. Zhang, Y. Wang, C. Wolf, H. Aubin, A. Heinrich and T. Choi, *ACS Nano*, 2021, **15**, 17959–17965.
31 A. L. Linsebigler, G. Lu and J. T. Yates, *Chem. Rev.*, 1995, **95**, 735–758.
32 Y. Sari, P. L. Gareso, B. Armynah and D. Tahir, *Int. J. Hydrogen Energy*, 2024, **55**, 984–996.
33 S. A. Chambers, S. Thevuthasan, R. F. C. Farrow, R. F. Marks, J. U. Thiele, L. Folks, M. G. Samant, A. J. Kellock, N. Ruzycki, D. L. Ederer and U. Diebold, *Appl. Phys. Lett.*, 2001, **79**, 3467–3469.
34 A. Omar, M. S. Ali and N. Abd Rahim, *Sol. Energy*, 2020, **207**, 1088–1121.
35 J. Zhao, H. Wang, Y. Cai, J. Zhao, Z. Gao and Y.-Y. Song, *ACS Sens.*, 2024, **9**, 1644–1655.
36 S. Hussain, C. Cao, Z. Usman, Z. Chen, G. Nabi, W. S. Khan, Z. Ali, F. K. Butt and T. Mahmood, *Thin Solid Films*, 2012, **522**, 430–434.
37 D. Joshy, S. B. Narendranath, Y. A. Ismail and P. Periyat, *Nanoscale Adv.*, 2022, **4**, 5202–5232.
38 I. Ali, M. Suhail, Z. A. Alothman and A. Alwarthan, *RSC Adv.*, 2018, **8**, 30125–30147.
39 U. Diebold, *Surf. Sci. Rep.*, 2003, **48**, 53–229.
40 F. Sedona, G. A. Rizzi, S. Agnoli, F. X. Llabrés i Xamena, A. Papageorgiou, D. Ostermann, M. Sambi, P. Finetti, K. Schierbaum and G. Granozzi, *J. Phys. Chem. B*, 2005, **109**, 24411–24426.
41 S. Agnoli, T. Orzali, M. Sambi, A. Vittadini, M. Casarin and G. Granozzi, *J. Phys. Chem. C*, 2008, **112**, 20038–20049.
42 G. T. Harrison, M. C. Spadaro, C. L. Pang, D. C. Grinter, C. M. Yim, P. Luches and G. Thornton, *Mater. Sci. Technol.*, 2016, **32**, 203–208.
43 S. Tosoni and G. Pacchioni, *J. Phys. Chem. C*, 2019, **123**, 7952–7960.
44 K. G. Reeves, J. Ma, M. Fukunishi, M. Salanne, S. Komaba and D. Dambournet, *ACS Appl. Energy Mater.*, 2018, **1**, 2078–2086.
45 F. Rossella, P. Galinetto, M. C. Mozzati, L. Malavasi, Y. Diaz Fernandez, G. Drera and L. Sangaletti, *J. Raman Spectrosc.*, 2009, **41**, 558–565.
46 A. L. Sorrentino, G. Serrano, L. Poggini, B. Cortigiani, K. E. El-Kelany, M. D'Amore, A. M. Ferrari, A. Atrei, A. Caneschi, R. Sessoli and M. Mannini, *J. Phys. Chem. C*, 2021, **125**, 10621–10630.
47 A. L. Sorrentino, I. Cimatti, G. Serrano, L. Poggini, B. Cortigiani, L. Malavolti, E. Otero, P. Sainctavit, M. Mannini, R. Sessoli and A. Caneschi, *J. Mater. Chem. C*, 2021, **9**, 15011–15017.
48 A. Cornia, M. Mannini, R. Sessoli and D. Gatteschi, *Eur. J. Inorg. Chem.*, 2019, **2019**, 552–568.
49 L. Margheriti, M. Mannini, L. Sorace, L. Gorini, D. Gatteschi, A. Caneschi, D. Chiappe, R. Moroni, F. B. de Mongeot, A. Cornia, F. M. Piras, A. Magnani and R. Sessoli, *Small*, 2009, **5**, 1460–1466.
50 S. Ninova, V. Lanzilotto, L. Malavolti, L. Rigamonti, B. Cortigiani, M. Mannini, F. Totti and R. Sessoli, *J. Mater. Chem. C*, 2014, **2**, 9599–9608.
51 L. Malavolti, V. Lanzilotto, S. Ninova, L. Poggini, I. Cimatti, B. Cortigiani, L. Margheriti, D. Chiappe, E. Otero,

P. Sainctavit, F. Totti, A. Cornia, M. Mannini and R. Sessoli, *Nano Lett.*, 2015, **15**, 535–541.
52 P. Erler, P. Schmitt, N. Barth, A. Irmler, S. Bouvron, T. Huhn, U. Groth, F. Pauly, L. Gragnaniello and M. Fonin, *Nano Lett.*, 2015, **15**, 4546–4552.
53 L. Gragnaniello, F. Paschke, P. Erler, P. Schmitt, N. Barth, S. Simon, H. Brune, S. Rusponi and M. Fonin, *Nano Lett.*, 2017, **17**, 7177–7182.
54 F. Paschke, P. Erler, V. Enenkel, L. Gragnaniello and M. Fonin, *ACS Nano*, 2019, **13**, 780–785.
55 V. Lanzilotto, L. Malavolti, S. Ninova, I. Cimatti, L. Poggini, B. Cortigiani, M. Mannini, F. Totti, A. Cornia and R. Sessoli, *Chem. Mater.*, 2016, **28**, 7693–7702.
56 U. Diebold and T. E. Madey, *Surf. Sci. Spectra*, 1996, **4**, 227–231.
57 W. S. Oh, C. Xu, D. Y. Kim and D. W. Goodman, *J. Vac. Sci. Technol., A*, 1997, **15**, 1710–1716.
58 M. Oku, K. Wagatsuma and S. Kohiki, *Phys. Chem. Chem. Phys.*, 1999, **1**, 5327–5331.
59 K. S. Kim and N. Winograd, *Chem. Phys. Lett.*, 1975, **31**, 312–317.
60 S. K. K. Sen, J. Riga and J. Verbist, *Chem. Phys. Lett.*, 1976, **39**, 560–564.
61 J. T. Mayer, U. Diebold, T. E. Madey and E. Garfunkel, *J. Electron Spectrosc. Relat. Phenom.*, 1995, **73**, 1–11.
62 M. J. Jackman, A. G. Thomas and C. Muryn, *J. Phys. Chem. C*, 2015, **119**, 13682–13690.
63 W. S. Epling, C. H. F. Peden, M. A. Henderson and U. Diebold, *Surf. Sci.*, 1998, **412–413**, 333–343.
64 G. Serrano, A. L. Sorrentino, L. Poggini, B. Cortigiani, C. Goletti, R. Sessoli and M. Mannini, *Phys. Chem. Chem. Phys.*, 2021, **23**, 12060–12067.
65 A. Atrei, A. M. Ferrari, P. Finetti, A. Beni and G. Rovida, *J. Phys. Chem. C*, 2009, **113**, 19578–19584.
66 P. Finetti, M. Caffio, B. Cortigiani, A. Atrei and G. Rovida, *Surf. Sci.*, 2008, **602**, 1101–1113.
67 G. Liu, A. Klein, A. Thissen and W. Jaegermann, *Surf. Sci.*, 2003, **539**, 37–48.
68 L. Rigamonti, M. Piccioli, L. Malavolti, L. Poggini, M. Mannini, F. Totti, B. Cortigiani, A. Magnani, R. Sessoli and A. Cornia, *Inorg. Chem.*, 2013, **52**, 5897–5905.
69 P. Gobbo, M. C. Biesinger and M. S. Workentin, *Chem. Commun.*, 2013, **49**, 2831–2833.
70 H. Bennettand, G. J. O. Wiley, A. Benninghoven, K. T. F. Janssen, J. Tumpner and H. W. Wer, *J. Chem. Educ.*, 1993, **70**, A25.
71 L. Poggini, A. Lunghi, A. Collauto, A. Barbon, L. Armelao, A. Magnani, A. Caneschi, F. Totti, L. Sorace and M. Mannini, *Nanoscale*, 2021, **13**, 7613–7621.
72 C. J. Powell, *J. Electron Spectrosc. Relat. Phenom.*, 2012, **185**, 1–3.
73 J.-P. Kappler, E. Otero, W. Li, L. Joly, G. Schmerber, B. Muller, F. Scheurer, F. Leduc, B. Gobaut, L. Poggini, G. Serrano, F. Choueikani, E. Lhotel, A. Cornia, R. Sessoli, M. Mannini, M.-A. Arrio, Ph. Sainctavit and P. Ohresser, *J. Synchrotron Radiat.*, 2018, **25**, 1727–1735.
74 M. Mannini, E. Tancini, L. Sorace, P. Sainctavit, M.-A. Arrio, Y. Qian, E. Otero, D. Chiappe, L. Margheriti, J. C. Cezar, R. Sessoli and A. Cornia, *Inorg. Chem.*, 2011, **50**, 2911–2917.
75 L. Poggini, E. Tancini, C. Danieli, A. L. Sorrentino, G. Serrano, A. Lunghi, L. Malavolti, G. Cucinotta, A. L. Barra, A. Juhin, M. A. Arrio, W. Li, E. Otero, P. Ohresser, L. Joly, J. P. Kappler, F. Totti, P. Sainctavit, A. Caneschi, R. Sessoli, A. Cornia and M. Mannini, *Adv. Mater. Interfaces*, 2021, **2101182**, 1–9.
76 N. Giaconi, A. L. Sorrentino, L. Poggini, M. Lupi, V. Polewczyk, G. Vinai, P. Torelli, A. Magnani, R. Sessoli, S. Menichetti, L. Sorace, C. Viglianisi and M. Mannini, *Angew. Chem., Int. Ed.*, 2021, **60**, 15276–15280.
77 K. Kuepper, C. Taubitz, D. Taubitz, U. Wiedwald, A. Scheurer, S. Sperner, R. W. Saalfrank, J.-P. Kappler, L. Joly, P. Ziemann and M. Neumann, *J. Phys. Chem. Lett.*, 2011, **2**, 1491–1496.
78 P. Palmgren, S. Yu, F. Hennies, K. Nilson, B. Åkermark and M. Göthelid, *J. Chem. Phys.*, 2008, **129**, 074707.
79 P. Palmgren, B. R. Priya, N. P. P. Niraj and M. Göthelid, *Sol. Energy Mater. Sol. Cells*, 2006, **90**, 3602–3613.
80 E. Tancini, M. Mannini, P. Sainctavit, E. Otero, R. Sessoli and A. Cornia, *Chem. – Eur. J.*, 2013, **19**, 16902–16905.
81 M. J. Rodriguez-Douton, M. Mannini, L. Armelao, A.-L. Barra, E. Tancini, R. Sessoli and A. Cornia, *Chem. Commun.*, 2011, **47**, 1467–1469.
82 S. Tosoni and G. Pacchioni, *J. Phys. Chem. C*, 2020, **124**, 20960–20973.
83 H. Yanagi, S. Chen, P. A. Lee, K. W. Nebesny, N. R. Armstrong and A. Fujishima, *J. Phys. Chem.*, 1996, **100**, 5447–5451.
84 P. Palmgren, K. Nilson, S. Yu, F. Hennies, T. Angot, J. M. Layet, G. Le Lay and M. Gothelid, *J. Phys. Chem. C*, 2008, **112**, 5972–5977.
85 S. Yu, S. Ahmadi, P. Palmgren, F. Hennies, M. Zuleta and M. Göthelid, *J. Phys. Chem. C*, 2009, **113**, 13765–13771.
86 S. Yu, S. Ahmadi, C. Sun, P. Palmgren, F. Hennies, M. Zuleta and M. Göthelid, *J. Phys. Chem. C*, 2010, **114**, 2315–2320.
87 L. Cao, Y. Wang, J. Zhong, Y. Han, W. Zhang, X. Yu, F. Xu, D. C. Qi and A. T. S. Wee, *J. Phys. Chem. C*, 2011, **115**, 24880–24887.
88 V. Lanzilotto, G. Lovat, G. Fratesi, G. Bavdek, G. P. Brivio and L. Floreano, *J. Phys. Chem. Lett.*, 2015, **6**, 308–313.
89 S. C. Li, L. N. Chu, X. Q. Gong and U. Diebold, *Science*, 2010, **328**, 882–884.
90 P. Ohresser, E. Otero, F. Choueikani, K. Chen, S. Stanescu, F. Deschamps, T. Moreno, F. Polack, B. Lagarde, J.-P. Daguerre, F. Marteau, F. Scheurer, L. Joly, J.-P. Kappler, B. Muller, O. Bunau and P. Sainctavit, *Rev. Sci. Instrum.*, 2014, **85**, 013106.
91 G. Cucinotta, pyDichroX, Available at: **https://github.com/BeppeC/pyDichroX**.
92 M. W. Haverkort, M. Zwierzycki and O. K. Andersen, *Phys. Rev. B: Condens. Matter Mater. Phys.*, 2012, **85**, 165113.